JOURNAL OF CATALYSIS 157, 133–144 (1995)

A Method for Accurate Quantitative XPS Analysis of Multimetallic or Multiphase Catalysts on Support Particles

A. Frydman,*‡ D. G. Castner,† M. Schmal,‡ and C. T. Campbell*,[1]

*Department of Chemistry and †Department of Chemical Engineering, University of Washington, Seattle, Washington 98195-1750; and ‡NUCAT/COPPE/PEQ, Universidade Federal do Rio de Janeiro, CP 68502, CEP 21945, Ilha do Fundão, Rio de Janeiro, Brazil

Received November 9, 1994; revised June 13, 1995; accepted July 24, 1995

A mathematical formalism for the quantitative analysis of X-ray photoelectron spectroscopy (XPS) intensities for supported, multiphase catalysts is presented. Such powdered catalysts are modeled as spherical support particles, covered in regions (islands) by different stratified layers of phases. It specifically considers the variation in photoelectron take-off angle over the surface of the particles, by integrating the signal over the particle's volume. The evaluation of this integral can be done numerically, but for certain particle sizes it is simplified by a new approximation to the exponential integral function presented here, which introduces an error of <4%. The results show that the common assumption of normal emission usually leads to large errors (factors of 2–5). A simpler approximation to this new formalism, using the unweighted average take-off angle of photoelectrons from the local surface normal of 57.3°, introduces an error of <23% *except* for species whose main intensity arises from an underlayer that is buried by another phase of average depth greater than 1.3 λ (λ is a photoelectron's inelastic mean free path). It is useful for the initial optimization of parameters when searching for structural models of catalysts that are consistent with their XPS spectra. These formalisms are also applicable in treating other shapes of catalysts than those treated explicitly here, provided the phase's surface-to-volume ratio is the same as chosen in this model and that the BET surface area is less than about 35 m^2/g. More complex expressions which treat higher surface area samples are also presented. The formalisms can also be used in quantitative Auger electron spectroscopy (AES), if the XPS sensitivity factors are replaced by AES sensitivity factors. © 1995 Academic Press, Inc.

I. INTRODUCTION

Formulae for calculating the X-ray photoelectron spectroscopy (XPS) signals from supported catalysts have been presented previously in a number of papers (1–7). These papers agree that that XPS signal from a species, i, due to a differential volume element, $dxdydz$, at some depth, z, below the surface of a particle in a powdered sample is proportional to the probability, p, that a photoelectron of that species created in that volume element will escape without loss of energy through that particle's surface into the direction of the XPS analyzer. Neglecting elastic scattering, this probability is given by (8):

$$p = \exp[-z/(\lambda \cdot \cos\theta)], \qquad [1]$$

where λ is the inelastic mean free path (IMFP) of a photoelectron from orbital j of element i and is a function of the kinetic energy (KE) of the emitted photoelectron (8), and θ is the photoelectron's take-off angle into the analyzer, relative to the local surface normal of the particle. In calculating the XPS signal, p must be multiplied by $n_i(z)$, the atomic concentration of element i at depth z below the local surface (in units of atoms/cm^3), and this product must be properly integrated over the surface of the particles and through the depth (1, 8).

For powdered samples, the take-off angle, θ, varies from 0° to 90° in this integral. The full evaluation of this double integral is therefore complex, but it can in principle be performed numerically if the exact geometric structure of the powder is known. To overcome this difficulty, many authors have assumed that the take-off angle is zero (2–5). Davis (6) showed that this can lead to large errors, and developed a model where the catalyst particles were assumed to be diamond-shaped and oriented such that the take-off angle from each diamond face was 45°. Our purposes here are to:

(1) present geometric analogues to powdered samples which make this integration possible,

(2) determine if there exists an average take-off angle which would be more appropriate than 45° for powdered samples like supported catalysts, and

(3) incorporate these results into equations that would be appropriate for accurate quantitative estimates of XPS signals from supported bimetallic catalysts, yet for certain particle sizes are nearly as simple as those which result from the assumption that $\theta = 0$.

[1] To whom correspondence should be addressed.

0021-9517/95 $12.00

To our knowledge, only Kuipers *et al.* (1) and Cimino *et al.* (7) have previously addressed this issue of properly integrating over the take-off angles, θ, in a powdered or "random" sample of a supported catalyst. Kuipers *et al.* (1) began with a beautiful and simple set of statements as a starting point: "For true random samples every orientation angle of a surface element in space is of equal probability. This statement has a geometric analogue, namely that the surface of a random sample may be represented by a hemisphere." They went on to calculate the signal ratio between a photoelectron line for a supported catalyst material, k, and a line for its support material, s, for a random or powdered sample, by averaging via integration over the whole possible range of surface orientation angles with respect to the analyzer axis. They assumed several different geometries for the catalyst phase, including a thin, flat layer, spherical particles, and hemispherical particles. Unfortunately, they only derived mathematical formulae for samples like monometallic supported catalysts, where the powdered compound has only one other compound or phase, like a metal catalyst, supported on its surface. However, their formalism can be extended easily to multimetallic, multiphase, multilayered samples, as we will show here. Cimino *et al.* (7) also treated only monometallic supported catalysts. They approximately integrated the signal over the surface of a hemisphere by summing over four concentric surface regions, using the equivalent of an average take-off angle within each region.

We are interested in multimetallic catalysts that might have layered overlayer phases or layered particles supported on the surface of a powdered oxide or other powdered material. For example, supported CuRu bimetallic catalysts might have surface-segregated Cu on top of Ru in the supported metal particle sitting on an oxide support. Therefore we require a more general formalism, which we present here. It is, mathematically, an extension of the "randomly oriented layer" model of Kuipers *et al.* (1), except that it explicitly considers multilayered supported catalysts, and it has as its basis a different physical picture. The formulae in both models are most accurately solved by full numerical integration. To make this integration simpler, we also present approximate analytical expressions for the exponential integral function. In addition, we show that the "randomly oriented layer" formalism of Kuipers *et al.* (1), upon which our formalism is based, incorporates a certain unstated assumption which leads to large inaccuracies when the support particles are small or even for large particles if the overlayer phase is thick. We will estimate the magnitude of this error and present a formula here which corrects that error. Finally, we present here a far simpler but more approximate method that has sufficient accuracy for some applications, especially for making first estimates of parameters in structural models of catalysts that match their XPS spectra.

We will model the catalyst here as being supported on spherical particles, and the active overlayer phases as a sequence of stratified layers, each of uniform thickness, covering certain fractions of these spheres in a certain stacking order. The resulting formalisms should be more generally applicable than this stratified, partial spherical shell model implies because, as beautifully shown by Kuipers *et al.* (1): "For truly random samples, the XPS signal of a supported phase which is present as equally sized but *arbitrarily shaped convex particles* is determined by their surface to volume ratio." Thus, any catalyst particle or supported island shapes that have the same total surface area to volume ratios and the same total volume as chosen in this model should give similar XPS signals.

II. THE MODELS

II.1. Flat Samples

We start with the traditional equation for flat samples that describes the photoelectron intensity due to the integrated depth distribution of the element, weighted by the exponential decay of the escape probability of emitted photoelectrons with sampling depth (Eq. [1]) (8–10). The integrated XPS intensity from the analysis area A of a flat sample for orbital j of element i is given by

$$I_{ij} = L_{ij}(\gamma)\,\sigma_{ij} K T_{KE} A \int_{z=0}^{\infty} n_i(z) \exp[-z/(\lambda \cdot \cos\theta)]\, dz, \quad [2]$$

where

$L_{ij}(\gamma)$ is the angular asymmetry factor of orbital j of element i;

σ_{ij} is the photoionization cross section of orbital j of element i, taken from (11);

K is an instrumental constant which depends on the intensity and incident angle of the X-ray source;

T_{KE} is the transmission probability of the XPS analyzer which is a smooth function of the kinetic energy (KE) of the emitted photoelectron and which can depend on the geometry and pass energy of the analyzer, but for a given geometry and KE, it is assumed here to be a constant within the analysis area and zero elsewhere;

$n_i(z)$ is the atomic concentration of element i at depth z below the local surface (in units of atoms/cm^3);

λ is the inelastic mean free path of a photoelectron from orbital j of element i which is a function of the kinetic energy of the emitted photoelectron, and may depend on the material, taken from Tanuma *et al.* (12); and

θ is the photoelectron polar take-off angle relative to the local surface normal.

With this set of definitions, the product $K \cdot T_{KE} \cdot A$ will

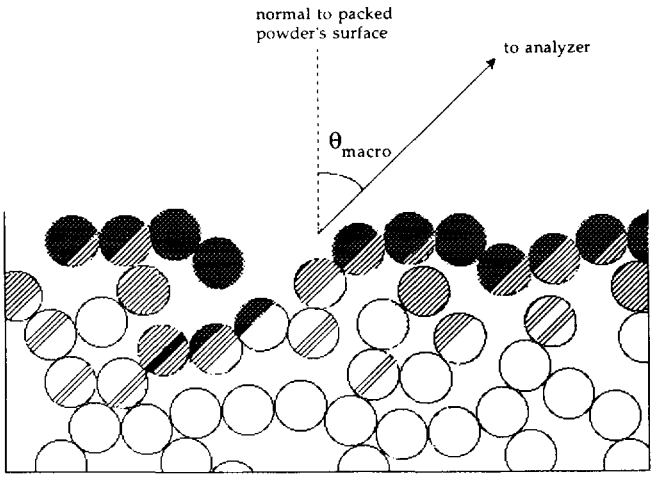

FIG. 1. Schematic representation of a powdered sample as a set of equally sized spheres. The set of volumes which constitute the topmost layer of spheres is shown in black, and the second layer volume is shown as shaded areas. Since the volumes in each layer are randomly chosen, each layer sums up to a complete set of spheres.

grow as $1/\cos\theta$ in the case of a large-spot X-ray source and a large sample, because the analysis area A will increase in this way. It will not vary with θ for X-ray spots or samples that are smaller than A. The angular asymmetry factor is unity for all elements in spectrometers which operate at a "magic angle," which is 54.7° between the X-ray and detected electron vectors when elastic electron scattering is neglected (16). When elastic electron scattering is included, the magic angle is somewhat larger (~63°) (16). As our spectrometer operates near this latter angle, we will treat this factor as unity here, although it can be easily included in the final equations we shall derive.

II.2. Powdered Samples: Spherical or Random Model

We consider next powders or random samples, which will be modeled here as a randomly located array of equally sized spheres, as shown in Fig. 1. The effective radius of the spheres can be estimated by equating their BET surface area per unit mass to that of the real catalyst. The XPS signal from such an array will accurately represent the signal from a real powdered catalyst of the same surface-to-volume ratio only if the radii of curvature presented in the real catalyst are not too different from this value (i.e., only if the particle size distribution is not too broad). We choose spherical particles since a spherical surface accurately represents the distribution of angles between the surface normal and the axis of the detector of a randomly oriented powder of arbitrary shape, as shown by Kuipers *et al.* (1). This is true since this probability distribution is constant (independent of angle) in both cases. Also, Kuipers *et al.* (1) showed for a variety of regularly shaped, equally sized, but randomly oriented convex particles (rectangles, hemispheres, and spheres) that the XPS signal from a fixed volume is a function of the surface-to-volume ratio, but independent of shape. Thus, one could reasonably expect that the signal from a single spherical particle could accurately represent that from part of a powdered sample carefully chosen to have the same volume and the same surface-to-volume ratio as the sphere. One should be able to keep choosing parts of the powder that match single spheres, until the whole powder has been modeled by this array of fixed diameter spheres. Again, this probably fails for powders made up of particles with a very broad distribution of sizes or surface curvatures.

First, we treat only spheres whose effective diameter is much larger than the escape depth of photoelectrons (typically 0.5–4 nm), so the attenuation of photoelectrons originating from one "sphere" by other "spheres" was considered to be complete. That is, the observed photoelectrons were assumed to arise from spheres on the very surface of the powder as mounted. While some spheres will be completely "seen" by a detector at large distance, other spheres in this array will be partially "masked" by other spheres that sit between it and the detector. However, since the packing is random, the probability that any given part of any given sphere be seen by the detector is equal. Since the parts of the spheres that are seen are randomly chosen, they sum together to make a complete set of spheres, as shown in Fig. 1. Thus, only one full and unmasked sphere needs to be considered to obtain the proper distribution of take-off angles. In effect, this means that the XPS intensities could be modeled by considering the photoelectron emission from a single, isolated sphere of a typical effective diameter into an analyzer at infinite distance. The curvature of the particle surfaces is not explicitly taken into consideration in any other way except by considering the variation in the take-off angle over the particle's surface. In this case, the XPS intensity in Eq. [2] above must be integrated over the volume of a spherical particle. Here, we will also assume that the particle is so big that no electrons can get to the spectrometer if they originate from the back surface of the particle. (Using typical densities and λ values, this means that the BET surface area must be less than about 35 m^2/g.) Thus, this integral must be performed only over the front half of the sphere. The intensity from one such outer hemisphere of radius, R, within the analysis area is just

$$I_{ij} = KT_{KE}\, L_{ij}(\gamma)\, \sigma_{ij} \int_{r=0}^{R} \int_{\theta=0}^{\pi/2} \int_{\phi=0}^{2\pi} n_i(r) \exp[-(R-r)/(\lambda \cdot \cos\theta)]\, r^2 \sin\theta\, dr\, d\theta\, d\phi, \quad [3]$$

where r is the radius from the center of the particle, θ is the polar angle measured from the direction to the ana-

lyzer, and ϕ is the azimuthal angle. The integral over ϕ just gives 2π. We consider first only particles whose radius, R, is much, much larger than λ, so that the integral really need only be performed over a film of thickness equal to about 5λ on the surface of the particle. In this case, the integral can be replaced with

$$I_{ij} = KT_{KE}\, L_{ij}(\gamma)\, \sigma_{ij}\, 2\pi R^2 \int_{z=0}^{\infty} \int_{\theta=0}^{\pi/2} n_i(z) \exp[-z/(\lambda \cdot \cos\theta)] \sin\theta\, dz\, d\theta, \quad [4]$$

where $z = R - r$ is the depth below the local surface of the particle. For simplicity, we let its upper limit go to infinity rather than just to 5λ, since the contribution to the integral between these limits is negligible (<1%).

II.3. Stratified Layers or Spherical Shells

Fitting data from flat samples with Eq. [2] is difficult, because there are an infinite number of functions $n_i(z)$ that might describe the depth distribution of an element i. To simplify this situation, one normally assumes stratified layers of known phases. That is, different phases, each with a specific thickness, are encountered as one looks deeper and deeper into the catalyst surface, but, within each phase, the concentration of element i is either zero or a constant characteristic of that phase. For a spherical particle instead of a flat sample, this is equivalent to assuming that it is made up of different phases, each of which is a concentric spherical shell.

When $n_i(z)$ assumes a constant value of N_i within some layer from z_1 to z_2, as suggested by this "spherical shell" model, then Eq. [4] reduces to

$$I_{ij} = KT_{KE}\, L_{ij}(\gamma)\, \sigma_{ij}\, 2\pi R^2 N_i \int_{z=z_1}^{z_2} \int_{\theta=0}^{\pi/2} \exp[-z/(\lambda \cdot \cos\theta)] \sin\theta\, d\theta\, dz. \quad [5]$$

Integrating over z gives

$$I_{ij} = KT_{KE}\, L_{ij}(\gamma)\, \sigma_{ij}\, 2\pi R^2 N_i \lambda \left\{ \int_{\theta=0}^{\pi/2} \exp[-z_1/(\lambda \cdot \cos\theta)] \sin\theta \cos\theta\, d\theta - \int_{\theta=0}^{\pi/2} \exp[-z_2/(\lambda \cdot \cos\theta)] \sin\theta \cos\theta\, d\theta \right\}. \quad [6]$$

To simplify evaluation of these integrals, we define the function E_3 of x as

$$E_3(x) = \int_{\theta=0}^{\pi/2} \exp[-x/\cos\theta] \sin\theta \cos\theta\, d\theta. \quad [7]$$

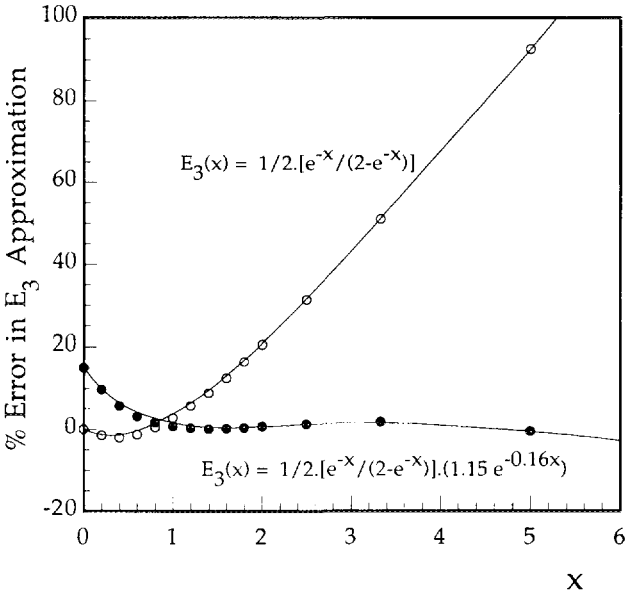

FIG. 2. Relative errors between different approximate expressions for the exponential integral function: Eq. [9] or Kuipers' approximate expression (1), open symbols; Eq. [10], filled symbols. When approximating the exponential integral function, one should use Eq. [9] when $x \leq 0.87$, and Eq. [10] for all larger x.

This function, $E_3(x)$, is equal to the well-known and tabulated (13) exponential integral function (1). With it, Eq. [6] simplifies to

$$I_{ij} = KT_{KE}\, L_{ij}(\gamma)\, \sigma_{ij}\, 2\pi R^2 N_i \cdot \lambda \cdot [E_3(z_1/\lambda) - E_3(z_2/\lambda)]. \quad (8)$$

Thus, calculating the angularly integrated signal from a layered phase near the surface of a sphere simply involves two evaluations of this function E_3.

The earlier paper on angle integration in XPS by Kuipers *et al.* (1) stated that $E_3(x)$ is reasonably approximated by

$$E_3(x) = \tfrac{1}{2} \exp[-x]/\{2\text{-}\exp[-x]\}. \quad [9]$$

We found that this approximation is acceptable *only* for $x < 1$. Its error grows rapidly with x for $x > 1$, reaching >20% by $x = 2$, and >90% already by $x = 5$. We have found a much better approximation for this integral when $x > 0.87$, given by

$$E_3(x) = \{\tfrac{1}{2} \exp[-x]/\{2\text{-}\exp[-x]\}\} \cdot \{1.15 \exp[-0.16x]\}. \quad [10]$$

The relative errors in these two approximations to the function E_3 are shown in Fig. 2, where the true value was taken from tables (13). As can be seen, if one uses Eq. [9] for $x \leq 0.87$ but Eq. [10] for $x > 0.87$, then the error will

always be quite acceptable (less than 4%) within the range of values of interest in evaluating Eqs. [5] or [8]: $x = z/\lambda < 6$. (The contribution to the XPS signal, or the value of E_3, is negligible deeper than this, so large percentage errors can be tolerated.) We recommend this combination of Eqs. [9] and [10], if numerical integration cannot be performed.

When possible, it is always advisable to do the full numerical integral. Approximations like this one for E_3 (i.e., using Eq. [9] for $x \leq 0.87$, but Eq. [10] for $x > 0.87$) are, however, useful time-saving devices. Short of doing the full numerical integration in solving Eq. [8] or any of Kuipers' equations for quantitative XPS (1), this new approximation should be used. It gives significantly improved accuracy compared to Eq. [9] alone when an overlayer is thicker than 1λ and covers more than a small fraction of the surface, or when a phase is buried by more than 1λ.

In more complex samples, element i may exist in more than one of the layers or spherical shells. In this case, one must take a sum of terms like that calculated in Eq. [8] for each shell where its concentration is nonzero.

II.4. The Average Take-Off Angle for Photoelectrons from Spherical Surfaces

We next show that Eq. [4] can be replaced by the simpler Eq. [2], provided a proper average polar take-off angle, θ_{av}, can be found. For this to be true, the following equality must hold:

$$A' \int_0^\infty n_i(z) \exp[-z/(\lambda \cdot \cos\theta_{av})]\, dz = 2\pi R^2 \int_{z=0}^{\infty} \int_{\theta=0}^{\pi/2} n_i(z) \exp[-z/(\lambda \cdot \cos\theta)] \sin\theta\, dz\, d\theta. \quad [11]$$

The analyzed area A' is just $2\pi R^2$ for this hemisphere. One must sum the signals from all hemispheres within the entire analysis area A to get the whole XPS signal. If $n_i(z)$ is known, Eq. [11] can then be solved for θ_{av}. It is clear that its value will depend on the exact form of $n_i(z)$. If the element is concentrated near the surface, the average take-off angle will be large; while if the element is deeply buried below the surface, it will only be seen for near normal emission. We have calculated θ_{av} with this equation, assuming that $n_i(z)$ is a constant in a concentric spherical shell between depth z_1 and z_2, and zero elsewhere. In this case, Eq. [8] can be used to evaluate Eq. [4]. The resulting average take-off angles are shown in Fig. 3 as a function of the average value of z/λ in the spherical shell, for various spherical shell thicknesses. As can be seen, the average photoemission angle assumes values from 90° to ~45°. The value of 45° assumed by Davis (6) is only accurate for deeply buried layers.

The reader should remember that the real surface area

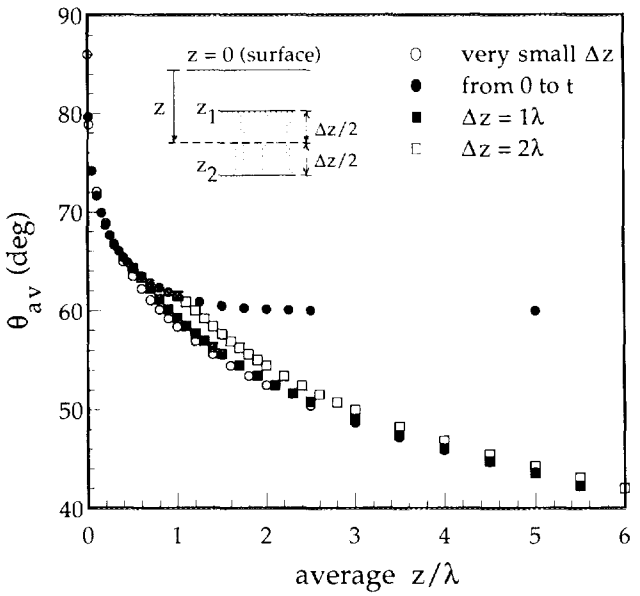

FIG. 3. Properly weighted average take-off angle of photoelectrons, relative to the local surface normal, from a spherical shell on the surface of a spherical particle, for various shell thicknesses, Δz. It is plotted here as a function of the average shell depth, z, relative to the inelastic mean free path of the electron, λ. (See inset for geometric explanation of z and Δz, where the shell of interest is shown as the shaded volume.) The filled egg-shaped symbols are for a shell which starts at the surface and extends a thickness t into the sample, such that the average z/λ is simply $t/2$. By definition, application of this angle in Eq. [2] for a slab model leads to the exact same results as Eq. [8] for such spherical shells.

seen by the XPS spectrometer is about twice as large for a powdered sample made up of large spherical particles as for a truly flat sample, provided that the spheres are packed thickly, such that gaps between spheres are filled by spheres below. This is because the analyzed area, A', of a sphere is $2\pi R^2$, but this sphere only occupies a *planar* area πR^2 across the analysis region, A. Thus, the inherent XPS signal from a powdered sample will be twice as large as that from a flat sample with the same depth distribution of elements, except for possible changes in intensity due to differences in the average take-off angles between the two types of samples, as quantified above.

The *geometrically* averaged take-off angle from the front surface of a sphere into a detector at infinite distance, unweighted by escape probabilities, is 57.3°. (We calculated this by integrating θ over this surface, and dividing by its area.) It turns out that using this single value in Eq. [2] gives a reasonable approximation to Eqs. [4] or [8] for a large range of layered structures on spherical surfaces. This can be seen in Fig. 4, where the relative error in this approximation, compared to the result from Eq. [8], is plotted for the same layered structures as were treated in Fig. 3. The relative error is always less than ~23% *except* for those layers which are buried by other material whose

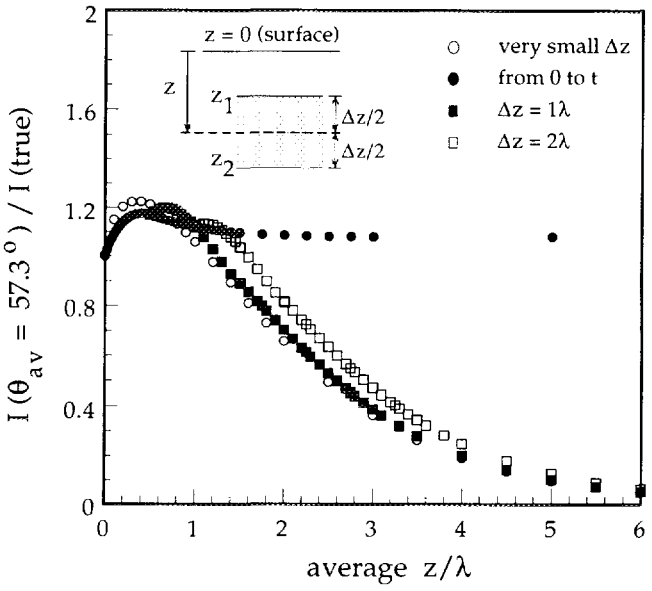

FIG. 4. This plot demonstrates the errors that result from a simple model where a single average take-off angle of 57.3° is used with Eq. [2] for modeling the XPS signal from spherical shells on spherical particles. The ratio of the intensity calculated with this method, $I(\theta_{av} = 57.3°)$, to that calculated using the full double integral via Eq. [8], I(true), is plotted as a function of the average shell depth, z, relative to the inelastic mean free path of the electron, λ, for various spherical shell thicknesses. (See Fig. 3 for definitions of z, Δz and t.)

thickness is bigger than about 1.3 λ. In real supported catalysts, the main contribution to the XPS signal from any one element is frequently *not* due to such deeply buried layers, so the use of 57.3° is often quite reasonable. While it is true that the support material is often covered in patches by layers of the active catalyst that are thicker than 1.3 λ, the fraction of the support that is covered by these patches is often small. While 23% is an unacceptable error in many applications, it is acceptable in others. Such quick but very approximate methods are, for example, quite useful in the preliminary optimization of structural parameters in structural models for catalysts that match their XPS spectra, as we have shown elsewhere (14).

Frequently, powdered samples are analyzed with models where the average take-off angle is assumed to be normal to the local surface, or 0° (2–5). It is useful to see how this compares to the methods we describe above. Figure 5 shows the same type plot as Fig. 4, only here $\theta_{av} = 0°$ was used. Thus, the error in the calculated intensity using this approximation, relative to full angular integration, is plotted for the same series of layered structures (spherical shells) as modeled in Fig. 4. As can be seen, the error in assuming 0° is always very large (>50%) whenever the average depth of the layer is greater than λ/2. This approximation generally does much worse than the 57.3° approximation.

One can see from Fig. 3 that 57.3° more closely approximates the true average angle than does Davis' model, which assumes $\theta_{av} = 45°$ (6), except in cases with deeply buried layers. For such layers, which are rare in real catalysts, 45° is better. These comparisons highlight the importance of the present full integration methods, and the value of the approximate method using 57.3°.

Using $\theta_{av} = 57.3°$, or preferably taking θ_{av} from Fig. 2, allows one to use Eq. [2] instead of the more complex Eq. [4] or [8] in calculating XPS signals for powdered samples provided element i has a depth distribution that can be represented by a constant-concentration spherical shell. One can also apply this method to any concentration profile, provided one applies it shellwise, choosing spherical shell widths, Δz, small enough so that this condition holds within each shell and then summing signals from the shells. Alternatively, one could also apply Eq. [8] shellwise. Both Eqs. [8] and [2] using θ_{av} from Fig. 2 are very accurate (<3%). The possible errors in the 57.3° approximation (Fig. 4) should be remembered when it is used. This approximation should not be used for deeply buried layers.

II.5. Layered Support Particles: The Partial, Stratified Spherical Shell Model

In real catalysts, different depth distributions of the elements, $n_i(z)$, exist on different regions of the support parti-

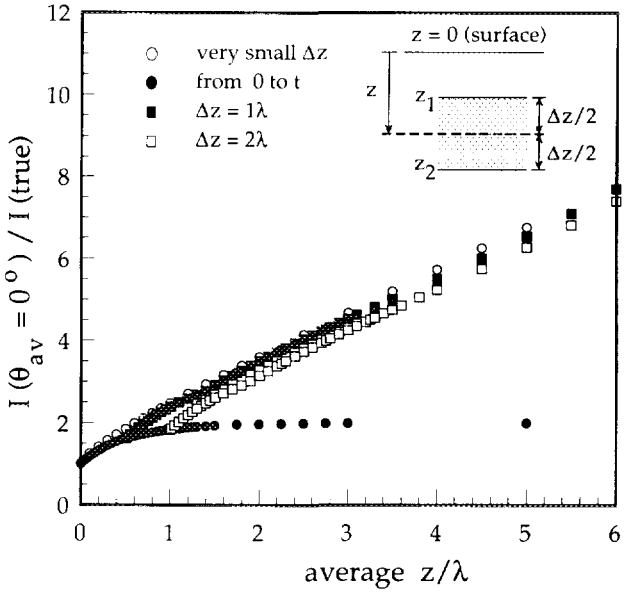

FIG. 5. This plot demonstrates the errors that result from a common model where a single average take-off angle of 0° is used with Eq. [2] for modeling the XPS signal from surface layers on spherical particles. The ratio of the intensity calculated with this method, $I(\theta_{av} = 0°)$, to that calculated using the full double integral or Eq. [8], I(true), is plotted as a function of the average shell depth, z, relative to the inelastic mean free path of the electron, λ, for various spherical shell thicknesses. (See Fig. 3 for definitions of z, Δz and t.)

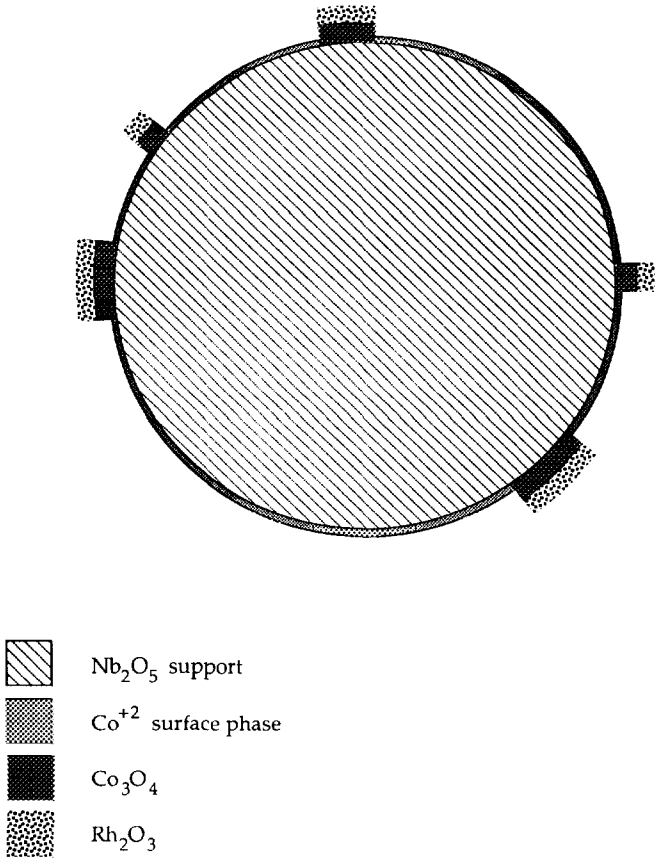

FIG. 6. Schematic representation of a typical catalyst structure that is based on the partial, stratified spherical shell model. This actually is the preferred structural model for a series of calcined Co–Rh/Nb_2O_5 catalysts we have studied elsewhere (14). This model has bilayer islands of Rh_2O_3 on Co_3O_4 covering a fraction f of the niobia support surface, with Rh_2O_3 on top, and a highly dispersed Co^{+2} phase covering all regions in between these islands.

cle's surface. For example, in supported monometallic catalysts the metals may exist as islands or supported particles on the support, where some regions of the support are covered by metal and others are not. Kuipers *et al.* (1) have treated these supported monometallic catalysts with a mathematical model equivalent to treating the metal phase as a partial spherical shell of uniform thickness which covers only a fraction of the surface of the inner, concentric support sphere. We extend their model here to include multiphase supported particles. We treat these as partial, stratified spherical shells over a spherical support particle. An example of such a model is shown schematically in Fig. 6. It turns out that this structure accurately represents a real calcined Co–Rh bimetallic catalyst on a niobia support which we have analyzed elsewhere using the equations presented here (14).

In evaluating the total XPS signal from such a complex sample using the above equations, a sum of terms must be taken for every region, k, of the sphere that has a different depth distribution. Thus, to calculate the total XPS intensity for level j of element i originating from one sphere, a sum of terms $I_{ij}(k)$ is taken, using Eq. [8] or Eq. [2] (with the proper θ_{av}) to evaluate each $I_{ij}(k)$:

$$I_{ij}(\text{sphere}) = \sum_k f_k \cdot I_{ij}(k). \qquad [12]$$

Here, f_k is the fraction of the support particle's surface covered by region k, and $\Sigma_k f_k = 1.0$. Within each region k, the depth variable z starts at zero from the *local* surface of the topmost layer when evaluating $I_{ij}(k)$. This equation assumes that the supported "particles" (or stratified, partial spherical shells) have a dimension parallel to the support surface that is large compared to the stratified layer thickness. We will argue below that this restriction is not actually necessary in applying this equation with accuracy, provided that the real supported islands have a uniform size distribution and that the model used for them based on these equations has the same total surface-to-volume ratio as the real particles.

Simple geometric formulae relate the thicknesses of phases, their densities, and the surface fractions covered by these phases with the total amounts of each element present in the catalyst. These mass balances bring important additional equations to the problem which must be satisfied, in addition to the XPS intensity equations, for any accurate structural model of the catalyst to truly fit the data. Examples of the use of such mass balances are presented in Ref. (14) for supported bimetallic catalysts where the active metals (Rh and Co) exist in three separate phases on niobia support particles.

II.6. Powdered Samples with Higher Surface Area

When a powdered sample has a very high surface area (>35 m^2/g), the effective radius of its spheres become comparable to λ, and several of the assumptions in the above derivations can lead to substantial errors. We first treat spheres that are still large enough that electrons from an underlying sphere have insignificant probability of passing through the overlying sphere. Even here, Eqs. [3] and [4] have approximations that fail when the radius of curvature is comparable to λ. First, the distance that a photoelectron originating at point (r, θ, ϕ) must travel through the solid is not simply $\{(R - r)/\cos\theta\}$ as implied by Eq. [3], but is really $\{\sqrt{(R^2 - r^2\sin^2\theta)} - r\cos\theta\}$. Also, r^2 is not exactly R^2, as implied by Eq. [4]. Note, however, that these both become good approximations when $(R - r)/R \ll 1$, which is the only region of interest when $R \gg \lambda$. Fortunately, these two approximations give errors with opposite signs on I_{ij}, so they cancel to some extent. To evaluate the magnitude of these errors, we have performed numerical

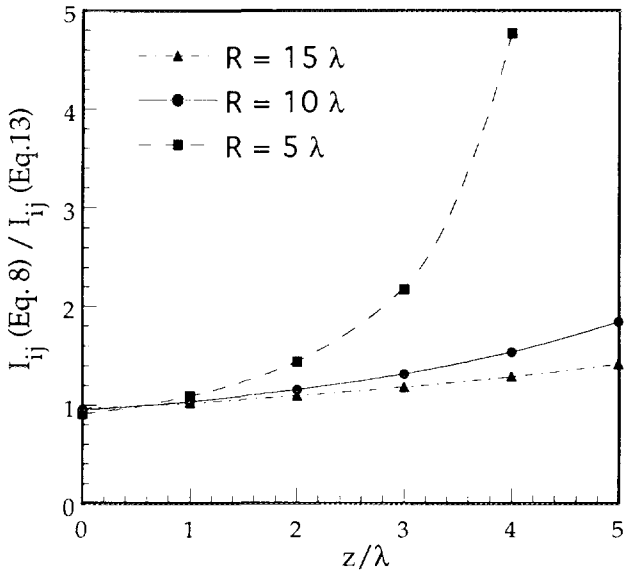

FIG. 7. A comparison of the XPS intensities calculated using Eq. [8] and the more accurate Eq. [13], for a very thin spherical shell of fixed concentration of element i within a concentric spherical particle, as a function of the shell's depth below the particle's surface, $z = R - r$. The comparison is presented for various particle radii, R, relative to the photoelectron's IMFP, λ.

integrations of the correct equivalent of Eq. [3], for comparison to the result from Eq. [4]. The correct equivalent to Eq. [3] is

$$I_{ij} = KT_{(KE)}\, L_{ij}(\gamma)\sigma_{ij} \cdot 2\pi \int_{r=0}^{R} \int_{\theta=0}^{\pi} n_i(r) \exp[-\{\sqrt{(R^2 - r^2 \sin^2\theta)} - r\cos\theta\}/\lambda] r^2 \sin\theta\, dr\, d\theta, \quad [13]$$

Here, $\{(R - r)/\cos\theta\}$ has been replaced with the accurate expression given above, and the limit on the θ integral has been increased from $\pi/2$ to π, so that the whole sphere, and not just the top hemisphere, is included. Again, the integral was performed numerically for a sperical shell of thickness Δz (or Δr) at average depth z ($R - r$) below the sphere's surface where there is a constant concentration, N_i (and zero concentration elsewhere). This is exactly what was done in Figs. 2–4, except here we use Eq. [13] instead of Eq. [4] or its equivalent for this geometry, Eq. [8]. Only very thin shells were studied, exactly like those in the open oval symbols of Figs. 2–4. The results are shown in Fig. 7, where the ratio of the XPS intensity calculated using Eq. [8] to the intensity using Eq. [13] is plotted as a function of z/λ, for several ratios of R/λ. As can be seen, Eq. [8] is fairly accurate when $R \geq 10\lambda$, except for deeply buried layers. However, Eqs. [8] and [4] are rather inaccurate whenever $R \leq 5\lambda$, unless the layer is not deeply buried. When Eq. [8] fails, it gives intensities that are too high due to the fact that R^2 is larger than r^2, and not equal as was assumed.

Thus, the formalisms in Sections II.2–II.5 are acceptable for effective spheres of radius greater than about 25 nm, for a typical λ of 2.5 nm. Using a typical oxide density of 3.5 g/cm^3, this corresponds to powders with specific surface areas below ~35 m^2/g. Equation [13] should be used for powders between ~35 and 100 m^2/g. Note that this equation can be applied to spherical shells of constant concentration to simplify the integral, and these terms can be summed via Eq. [12] to accurately treat partial spherical shells in this size regime. When the area exceeds ~350 m^2/g, most samples can be considered homogeneous in concentration, in which case the equations are trivial (8, 10). (If one element is tightly concentrated near the center of the spheres, the homogenous model is appropriate only for areas greater than ~700 m^2/g.)

For areas between ~100 and ~350–700 m^2/g, a formalism which explicitly considers the incomplete attenuation of electrons from one sphere by overlying spheres should be employed. Formalisms which consider this were previously presented by Kerkhoff and Moulijn (2) and by Kuipers *et al.* (1). The Kerkhoff formalism assumes normal emission, which can be grossly inaccurate as shown above. The model of Kuipers *et al.* properly averages over all emission angles. It explicitly considers only two-phase samples, but could be easily extended to multilayered samples. (Indeed, Eq. [8] above would be the central formula in such an extension.) However, Kuipers' formalism has a certain unstated assumption which leads to inaccuracy even in two-phase systems, as we will show below. This error arises from the fact that an equation equivalent to Eq. [8] is used in Kuipers's formulae, whereas Eq. [13] is more accurate for small particles for the reasons outlined above.

It is simple to correct Eq. [13] for the incomplete attenuation of electrons from one sphere by overlying spheres. We will treat the first layer of spheres at the surface exactly, using Eq. [13]. All underlying spheres will also be treated with this same equation to calculate the intensity I_{ij} emitted from that sphere toward the analyzer, only now this intensity will be attenuated by the overlying spheres. The first effective layer of spheres includes all parts of all particles which can emit electrons directly into the analyzer without passing through any other spheres (see black regions in Fig. 1). The second layer of spheres includes all parts of spheres which emit electrons directly into the analyzer while passing through only one other sphere (see shaded regions in Fig. 1). Each effective sphere in any layer occupies a planar area of $\pi R^2/\cos\theta_{macro}$ across the analyzed area A, where θ_{macro} is the angle between the analyzer axis and the normal to the macroscopic surface of the packed powder of spheres. Thus each effective layer of spheres includes a total number of spheres equal to $A/(\pi R^2/\cos\theta_{macro})$ within the analyzed area. Each sphere within the

first layer of spheres gives an intensity equal to that from Eq. [13], unattenuated by other spheres. The total intensity from the first layer is just this intensity times the number of spheres in this layer:

$$I_{ij,\text{layer 1}} = [A \cos \theta_{\text{macro}}/(\pi R^2)] \cdot [I_{ij}, \text{from Eq. [13]}]. \quad [14]$$

Each sphere within the second effective layer of spheres gives an intensity equal to that from Eq. [13], but now attenuated by a sphere of the first layer. An electron leaving a sphere in the second layer must pass through some length of solid in a sphere of the first layer. We will assume random packing of spheres, so that this electron has equal probability of passing through any part of the overlying sphere. In an unrelated derivation, Kuipers *et al.* (1) have shown that the intensity in such situations is reduced by the factor

$$\Omega(2R/\lambda) = 2(\lambda/2R)^2[1 - (2R/\lambda + 1) \cdot \exp(-2R/\lambda)], \quad [15]$$

which they call the "attenuation function for spheres." This is the escape probability of electrons through a sphere, assuming they are emitted randomly from the area directly below the sphere.

The signal I_{ij} from the third layer of spheres is attenuated by the square of this attenuation factor, $\Omega(2R/\lambda)^2$, and so forth. The net signal from all spheres is just the sum over all layers of the intensity from the spheres within that layer,

$$I_{ij,\text{TOT}} = [A \cos \theta_{\text{macro}}/(\pi R^2)] \cdot [I_{ij,\text{from Eq.[13]}}] \cdot \left[\sum_{n=0}^{\infty} \Omega(2R/\lambda)^n\right], \quad [16]$$

where n is an integer. Note that the summation here reduces to $1/[1 - \Omega(2R/\lambda)]$, since $\Omega(2R/\lambda)$ is always less than one. Thus, Eq. [16] simplifies to

$$I_{ij,\text{TOT}} = [A \cos \theta_{\text{macro}}/(\pi R^2)] \cdot [I_{ij,\text{from Eq. [13]}}] \div [1 - \Omega(2R/\lambda)]. \quad [17]$$

We now show that Eq. [17] reduces to the proper limits whenever $R \gg \lambda$ or $R \ll \lambda$. When $R \gg \lambda$, the signal all comes from the first layer and is simply given by Eq. [14], which is correct. When $R \ll \lambda$, the exponential attenuation factor in Eq. [13] is unity, and therefore Eq. [13] is simple to evaluate by

$$I_{ij} = KT_{(\text{KE})}L_{ij}(\gamma)\sigma_{ij}(4\pi R^3/3)N_i, \quad [18]$$

where N_i is the average concentration of element i within a sphere's volume. Furthermore, the summation in Eq. [16] reduces to $3\lambda/(4R)$ when $R \ll \lambda$. (The reader that tries to verify this limit should be careful to take enough terms, out to third order, in the series expansion for $\exp(-2R/\lambda)$ in calculating the limit of $\Omega(2R/\lambda)$.) Thus, the total intensity is just

$$I_{ij,\text{TOT}} = [A \cdot \cos \theta_{\text{macro}}/(\pi R^2)] \cdot [KT_{(\text{KE})}L_{ij}(\gamma)\sigma_{ij}(4\pi R^3/3)N_i] \cdot [3\lambda/(4R)]. \quad [19]$$

This simplifies to

$$I_{ij,\text{TOT}} = KT_{(\text{KE})}A \cdot L_{ij}(\gamma)\sigma_{ij}N_i\lambda \cdot \cos \theta_{\text{macro}}. \quad [20]$$

This is the standard result for homogeneous samples (8, 10), which can be easily obtained from Eq. [2]. (If a sample is porous, as in a powder, the values on N_i and λ in Eq. [2] must be decreased and increased, respectively, by a factor equal to the volume fraction of solid, or one minus its pore fraction, and these factors cancel.) Note that $K \cdot T_{(\text{KE})} \cdot A$ will change as $1/\cos \theta_{\text{macro}}$ for large-spot X-rays, as we noted just after presenting Eq. [2] above.

Thus, Eq. [17] is the true master equation, and it can be used for samples of any BET surface area.

In real catalysts, different depth distributions of the elements, $n_i(z)$, exist on different regions of the support particle's surface, as was mentioned in Section II.5. Of course to model such catalysts using Eq. [17], it must use a value for I_{ij} from Eq. [13] which properly accounts for each different depth distribution. To do this, results from Eq. [13] for the different regions may be combined in a summation identical to that in Eq. [12] of Section II.5.

III. DISCUSSION

To test our formalisms, we have compared the XPS intensities calculated using them with the results from Kuipers' formalism (1). This was done for several examples of supported monometallic catalysts, which is the most complex class of samples that can be handled by the formalism of Kuipers *et al.* (1) without further derivation. In these model systems, the support was assumed to be spherical particles of constant support element concentration, N_s, whose diameters were much larger than any electron inelastic mean free path. The active metal phase was assumed to be randomly spread as islands of constant thickness, t, and constant metal concentration, N_m, over a fraction, f, of the support surface. The surface otherwise was assumed to be clean. This model for monometallic catalysts is expressed by the combination of Eqs. [8] and [12]. Together, these give exactly the same formula for the XPS intensity ratio of the metal to a support element in such monometallic catalysts as in Kuipers' "randomly oriented layer model" (Eq. [7] from Ref. (1)), although the physical description of that model is quite different from ours. Indeed,

we found that the resulting metal:substrate XPS ratios from our full integration method, Eq. [8] with $z_1 = 0$ and $z_2 = t$, were within computer error (<1%) of the results applying numerical integration to Kuipers' equations for the whole range of t values when f was less than 10%. This is the situation in many supported catalysts. However, evaluating these integrals using Kuipers' approximate method for evaluating E_3 gives large errors (18–100%) whenever t is larger than 2λ and f is close to unity. These differences are only due to the inaccuracies in the evaluation of $E_3(x)$ using Kuipers' approximate method, or using Eq. [9] instead of Eq. [10] for $x > 0.87$. This situation occurs because the percentage errors in $E_3(t/\lambda)$ are large using Eq. [9] whenever t/λ exceeds 2, as was shown in Fig. 2.

Because Eq. [2] is equivalent to Eq. [8] when the true average angle from Fig. 3 is used, no further specific comparison of this second method with Kuipers' equation will be given here. The use of Eq. [2] with $\theta_{av} = 57.3°$ gave XPS ratios with small errors relative to using Kuipers' equation (with numerical integration). These errors were very close in magnitude to those plotted as egg-shaped symbols in Fig. 4, provided f was very small (<10%). When f and t were both large, this method was in serious error because the substrate was mainly buried. Thus, its signal incorporates the large errors shown by the open squares in Fig. 4, which arise for buried layers.

As stated above, Eqs. [8] and [12] above give the same mathematical formula for monometallic catalysts as the randomly oriented layer model of Kuipers *et al.* (1). Thus, the inaccuracies of Eq. [8] (or Eq. [4]) that occur for higher surface area powders, discussed in Section II.6 above, must also occur with the formulae of Kuipers *et al.*, although they do not point this out. For example, when the radius of curvature of the support particles becomes comparable to λ, there are errors in the method of calculating the distance photoelectrons must travel through the solid in both these models. There are other error factors as well, as discussed in Section II.6, where a more accurate formalism for such samples was presented.

It should be noted that we could have derived the equivalent of Eqs. [8] and [12] for multilayered, multimetallic catalysts following the derivation of the randomly oriented layer model of Kuipers *et al.* (1). However, we have chosen not to because that model presents a rather different physical picture of the catalyst than envisioned in our partial, stratified spherical shell model. Also, while the formulae resulting from these two models are the same when the particle radius is large compared to λ (i.e., for low-surface-area samples), they do differ markedly for high-surface-area samples, as we will show below.

Equation [17] above is the proper formula to apply for high-surface-area samples. Kuipers *et al.* (1) treated high-surface-area monometallic catalyst as well within their randomly oriented layers model, assuming a catalyst composed of a parallel array of support sheets, each of thickness t_s. The sample is composed of many such arrays of parallel sheets, and each array is randomly oriented with respect to the analyzer axis. Figure 8 compares the results of this formalism with our Eq. [17] for the case where $f_k = 1.0$, for a range of sample types and particle sizes. Here, the catalyst phase's shell thickness is called t_i, and the whole spherical particle's radius (support plus catalyst) is called R. In order to compare such physically different models, one must use a support layer thickness in Kuipers' model which is 2/3 the radius of our spherical support particles, r_s, as was pointed out by Kuipers *et al.* (1):

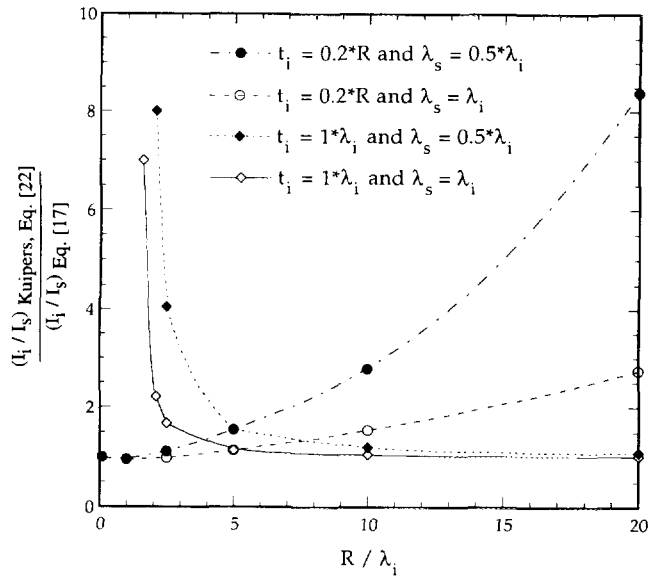

FIG. 8. A comparison of the XPS intensity ratio of catalyst to support, I_i/I_s, calculated with Eq. [22] from Kuipers *et al.* (1) and that calculated with our Eq. [17]. Here, t_i is the catalyst phase's shell thickness, R is the whole spherical particle's radius (support plus catalyst), and λ_s and λ_i refer to the inelastic mean free paths for the support and catalyst elements, respectively.

$$t_s = (2/3) \cdot r_s. \qquad [21]$$

This ensures that the support has the same surface:volume ratio in both models. Note that $R = r_s + t_i$, by definition. One must also ensure that the support and catalyst phases are present in the same volume ratio in both models. To do this, one must force the catalyst's phase thickness in Kuipers' model, t_k, to be equal to

$$t_k = (r_s/3) \cdot [(1 + t_i/r_s)^3 - 1]. \qquad [22]$$

(This correction highlights a certain difficulty associated with realizing the physical picture that underlies Kuipers' model. Thus, while the physical meaning of our t_i is obvi-

ous, that of t_k is not so clear.) Using these relations, Fig. 8 compares the XPS intensity ratio of catalyst to support, I_i/I_s, for two ratios of mean free paths: one where the support and catalyst phases have the same value (or $\lambda_s = \lambda_i$), and another where the value for the support is one-half that for the catalyst element (or $\lambda_s = \lambda_i/2$). The product $T_{(KE)}L_{ij}(\gamma)\sigma_{ij}$ was assumed to be the same for both elements and their elemental densities, n_i, within their respective phases were assumed to be the same. (These factors would cancel in *comparing* models anyway.) We used Eq. [22] from Kuipers *et al.* (1) in the calculation of Kuipers' model.

As can be seen in Fig. 8, Kuipers' model gives an XPS intensity ratio of catalyst to support, I_i/I_s, which is generally larger than that given by Eq. [17]. However, it works with high accuracy when the catalyst phase thickness is tiny, or when it is small compared to the particle radius R while R is larger than $\sim 10\lambda$. It is in serious error when either the catalyst phase has a thickness comparable to λ while R is less than $\sim 7\lambda$ or the catalyst phase thickness is a substantial fraction of R ($\geq 20\%$) while R is greater than about $\sim 5\lambda$. These errors in Kuipers' model occur because a certain assumption implicit in that model breaks down under these conditions. The origin of both these errors lies in the fact that, in the Kuipers model, the support is always treated as flat sheets, so that the escape path of a photoelectron through the solid from depth z below the surface is always $\{z/\cos\theta\}$, and not some smaller distance that takes into proper account the finite radius of curvature of the support. When their formulae are applied to spherical particles, they imply that a photoelectron originating at a point (r, θ, ϕ) within a sphere must travel through the solid particle a distance equal to $\{(R - r)/\cos\theta\}$ before exiting the particle toward the analyzer, as also implied by our Eqs. [3] and [8]. As we argued in Section II.6 above, however, this distance is really only $\{\sqrt{(R^2 - r^2\sin^2\theta)} - r\cos\theta\}$, as was incorporated in Eqs. [13] and [17]. This error is reflected in both Figs. 6 and 8. Note that the difference between t_i and t_k used above in applying Kuipers' equations to our structural model approximately corrects for the fact that r^2 in the region of interest is not exactly R^2, which is another assumption implicit in Eqs. [8] and [4], and reflected as error in Fig. 6. Thus, this part of the error in Fig. 6 does not appear in Fig. 8.

The errors in Kuipers' Eq. [22] are maximized in Fig. 8 because only full coverage ($\theta_k = 1.0$) was treated there. At smaller θ_k, the errors will be smaller. When θ_k is tiny, it is quite a good approximation even for a small R and a thick catalyst phase, since most of the support remains unburied (see the discussion regarding Fig. 7). Like our Eq. [8], Kuipers' Eq. [22] is only inaccurate when most of the signal from an element originates from well below the surface ($\sim\lambda$ or more, see Fig. 7).

The failures of the Kuipers model (their Eq. [22]) apparent in Fig. 8 will also occur when it is extended using their "sphere model," since their sphere model only changes the shape of the catalyst phase (from layers to spheres), but the support is still treated as flat sheets. If one went a step further and also treated the support as spheres within their formalism, this would simply require replacing their attenuation function Γ for the support in their Eq. [22] with the equivalent attenuation function for spherical supports (their Ω evaluated at $R_k = 3t_k/2$). Since Kuipers *et al.* (1) argue that Γ and Ω are nearly equal, one would not expect this to make much difference. We performed such calculations, and it does make some difference since Γ and Ω are not exactly the same. Nevertheless, the errors were just as large as, and generally larger than, those shown in Fig. 8.

This form of Kuipers' model does not give the same equations or intensity ratios as ours since their model implies that the catalyst phase is randomly spread over the *projected* area of the support spheres, and not randomly spread over the actual *surface* of the support spheres, as we assume. Since the face of a sphere contributes more to its projected area than its sides, this means that their model concentrates catalyst phase more on the face of the support sphere relative to the sides. This falsely weights the catalyst phase's spatial distribution in favor of locations with longer photoelectron travel lengths through the support. Also, Kuipers' model neglects "self-attenuation" by other catalyst spheres of the same layer, while our model does not. The extent of this self-attenuation is large for high coverages by the catalyst. Indeed, coverages by the catalyst of greater than 1/2 in Kuipers' spheres model do not make physical sense. (Note that their "apparent coverage" is greater than 1.0 in this case.)

Since no prior formalisms exist for more complex samples than the supported monometallic catalysts of the type discussed above, no comparison between our methods and other equations for multimetallic catalysts were possible. Elsewhere, we have demonstrated the utility of the formalisms presented here in quantitative interpretation of XPS spectra from real multiphase bimetallic catalysts (14). The catalysts analyzed were calcined cobalt/rhodium mixtures supported on macroporous niobia powder, modeled by 60-nm-diameter spheres to match its BET area. The structural model which best fit the bulk composition, XPS, and TPR data for these catalysts is shown schematically in Fig. 6. It has bilayer islands (~1–3 nm of Rh oxide on top of ~3–9 nm of Co_3O_4) covering a small fraction of the surface, with a submonolayer Co^{2+} phase everywhere in between these islands. By comparison to calculated intensities using Eq. [8], or full integration, we found that using Eq. [2] assuming a constant take-off angle of 57.3° was of sufficient accuracy to allow optimization of the structural parameters for this model (fraction covered and phase thicknesses). The Rh/Nb and Co/Nb XPS ratios agreed between the two methods to <9%. However, the XPS ratio of the two different phases

of cobalt ($Co^{2+}:Co_3O_4$) differed by 7 to 14%, depending on the Rh loading, between the two methods. This larger difference occurs because one of the Co phases is buried. The experimental error in this ratio, however, fell within these differences, so it was not a real problem in this particular case (14). In any case, this level of error shows that even this very approximate method using 57.3° is acceptable for the initial search of parameter space to find the right magnitude for initial guesses using the more accurate methods described above. Therefore, this quick method should be of general utility when trying to make initial guesses for structural parameters that match XPS spectra of catalysts.

The XPS signal from a random sample for a supported phase which is present as equally sized but *arbitrarily shaped* convex particles is determined entirely by their surface : volume ratio, as was so beautifully shown by Kuipers *et al.* (1). Therefore, the formulae derived here should also be rather generally applicable to shapes of catalyst phase particles other than those treated explicitly here. Specifically, they should accurately describe arbitrary convex shapes for the supported active phases' particles, provided that their real size distribution is narrow. However, for this to hold true, the partial spherical shell used to model them must be chosen so that it has their same total surface to volume ratio (and their same volume). Note that the total surface area here refers to the sum of the areas of all the particle surfaces, including the underlying support interface. Thus, one would get the same XPS signals from our partial spherical shell model with a catalyst phase of thickness t_i covering a fraction f_i of the support as with a model where the catalyst phase is composed of spheres of radius $3t_i/2$ covering a fraction $f_i/2$ of the support spheres, or of hemispheres of radius $9t_i/4$ covering a fraction of $2f_i/3$ of the support (see (1) for details).

While the above formalisms were derived with XPS in mind, they can also be used for AES, as long as the penetration depth of the incident electron beam is much larger than the inelastic mean free paths of the Auger electrons (17). Of course, one must substitute the proper AES sensitivity factors (15) in place of the product $L_{ij}(\gamma) \cdot \sigma_{ij} \cdot T_{(KE)} \cdot \lambda$ in the above equations.

The neglect of electron elastic scattering in Eq. [1] could lead to small errors in our formalisms here, as shown by Jablonski and Powell (17). When our formalisms are used to treat AES signals, these errors can be overcome by using the attenuation length in place of the inelastic mean free path (17). Such a straightforward correction is not possible in XPS (17).

ACKNOWLEDGMENTS

The authors thank the editor, Nick Delgass, and two conscientious referees of a previous paper (14) for very helpful comments that led to this paper. C.T.C. also warmly thanks H. P. C. E. Kuipers and C. J. Powell for helpful discussions. Financial support for this research by the Department of Energy, Office of Basic Energy Sciences, Division of Chemical Sciences is gratefully acknowledged by C.T.C.. A.F. thanks the CNPq (Conselho Nacional de Desenvolvimento Científico e Tecnológico), of the Secretary for Science and Technology of Brazil for the scholarship granted to pursue a split fellowship program at the University of Washington. A.F. also thanks Professor Márcia M. C. Ferreira (Department of Chemistry, UNICAMP, Brazil) for the assistance with the computer simulations.

REFERENCES

1. Kuipers, H. P. C. E., van Leuven, H. C. E., and Visser, W. M., *Surf. Interface Anal.* **8,** 235 (1986).
2. Kerkhoff, F. P. J. M., and Moulijn, J. A., *J. Phys. Chem.* **83,** 1612 (1979).
3. Angevine, P. J., Vartuli, J. C., and Delgass, W. N., *in* "Proceedings, 6th International Congress on Catalysis, London, 1976" (G. C. Bond, P. B. Wells, and F. C. Tompkins, Eds.), Vol. 2, p. 611. The Chemical Society, London, 1977.
4. (a) Linton, R. W., and Fulghum, J. E., *Surf. Interface. Anal.* **13,** 186 (1988); (b) Fung, S. C., *J. Catal.* **58,** 454 (1979).
5. Defossè, C., *J. Electron Spectrosc. Relat. Phenom.* **23,** 157 (1981).
6. Davis, S. M., *J. Catal.* **122,** 240 (1990); **117,** 432 (1989).
7. Cimino, A., Gazzoli, D., and Valigi, M., *J. Electron Spectrosc. Relat. Phenom.* **67,** 429 (1994).
8. Ertl, G., and Küppers, J., "Low Energy Electrons and Surface Chemistry," 2nd ed. VHC, Weinheim, 1985.
9. Ratner, B. D., and Castner, D. G., *in* "Surface Analysis and Its Applicatons," (J. C. Vickerman, ed.), Wiley, Chichester, U.K., in press.
10. Briggs, D., and Seah, M. P., Eds., "Practical Surface Analysis," 2nd ed., Vol. 1. Wiley Chichester, 1990.
11. Scofield, J. H., *J. Electron Spectrosc. Relat. Phenom.* **8,** 129 (1976).
12. Tanuma, S., Powell, C. J., and Penn, D. R., *Surf. Interface Anal.* **11,** 577 (1988); **17,** 911 (1991); **17,** 927 (1991); **20,** 77 (1993).
13. Abramovich, M., and Stegun, I. A., Eds., "Handbook of Mathematical Functions," U.S. National Bureau of Standards, Applied Mathematics Series 55, p. 228. U.S. Govt. Printing Office, Washington, DC, 1972.
14. Frydman, A., Castner, D. G., Schmal, M., and Campbell, C. T., *J. Catal.* **152,** 164 (1995).
15. Davis, L. E., MacDonald, N. C., Palmberg, P. W., Riach, G. E., and Weber, R. E., "Handbook of Auger Electron Spectroscopy," 2nd ed. Perkin–Elmer Corp., Minnesota, 1978; Payling, R., *J. Electron Spectrosc. Relat. Phenom.* **37,** 225 (1985).
16. Jablonski, A., and Powell, C. J., *Phys. Rev. B* **50,** 4739 (1994).
17. Jablonski, A., and Powell, C. J., *Surf. Interface Anal.* **20,** 771 (1993).